Modeling of Triblock Terpolymer Micelles with a Segregated Corona

Marat Charlaganov,*,†,‡ Oleg V. Borisov,‡,§ and Frans A. M. Leermakers†

Laboratory of Physical Chemistry and Colloid Science, Wageningen University, Dreijenplein 6, 6703 HB Wageningen, The Netherlands, Institute of Macromolecular Compounds, Russian Academy of Sciences, Bolshoi pr. 31, 199004 St. Petersburg, Russia, and Institut Pluridisciplinaire de Recherche sur l'Environnement et les Matériaux, F-64053 Pau Cedex, France

Received January 18, 2008; Revised Manuscript Received February 22, 2008

ABSTRACT: We report on self-consistent field predictions for the formation of spherical micelles by $A_NB_MC_N$ triblock terpolymers in a selective solvent, that is, a good solvent for the A_N and C_N blocks and a poor solvent for the middle B_M block. Above some threshold value for the repulsion between the *A* and *C* monomers, we find micelles with a laterally segregated corona, that is, Janus micelles. We consider the thermodynamic stability, the size, and the size fluctuations of these micelles. The transition between the homogeneous and the segregated states is smooth not only because of the finite size of the system, but also due to the compositional symmetry within the triblock terpolymer. It is found that the aggregation number decreases with increasing repulsion between *A* and *C* below the transition point and increases above the transition point. The formation of the interface is triggered by the high polymer density near the core. The interface between the *A* and *C* rich regions occupies a constant angle in spherical coordinates. This means that it widens in the radial direction. In these micelles, the lateral segregation gives a new fluctuation mode to the micelles; as the lateral segregation is coupled to the aggregation number, we anticipate a rich behavior in experimental systems.

Introduction

The field of molecular self-assembly has received continuous interest already over several decades.[1,2] The best known example is the micellization of short chain surfactants. The number of applications is many. They are used as detergents, in formulation science, and as wetting agents to name a few.[3] High molecular weight counterparts are increasingly studied because well-defined specimens are nowadays readily available. Much of what is known for surfactants is being applied to polymeric analogues.

Amphiphilic diblock copolymers are the simplest polymers able to form micelles. Similar to the case of low molecular weight surfactants, they feature a solvophobic block which escapes from the solvent and forms a dense core and a solvophilic block which accumulates on the outside and forms the corona. Simple geometric considerations indicate that when the aggregation number, that is, the number of molecules in the micelle, increases, the surface area per molecule decreases. As a result, the corona-forming block becomes stretched and this gives the main stopping mechanism for the assembly. The critical polymer concentration at which micelles start to form spontaneously (cmc) is typically very low.

There are several advantages of using polymeric micelles over surfactant ones.[4] From an application point of view, it is important that polymeric micelles are usually substantially larger than their low molecular weight analogues. For macromolecules, there exists a large degree of flexibility to choose the chemical composition of the blocks, resulting in weak to strong segregation of the solvophobic block with the solvent. Moreover, one can introduce chemical groups with tunable interactions and employ the cooperative nature of macromolecules to obtain responsive systems.

Recently, the self-assembly of *ABC* triblock terpolymers attracted substantial attention. In comparison with diblock copolymers, terpolymers offer additional flexibility for controlling the self-assembly process. They are known to demonstrate rich bulk phase behavior resulting in various microsegregated structures.[5] In solution, block terpolymers are able to form aggregates with complex morphology.[6−8] For example, the corona of a micelle formed by a double solvophilic terpolymer unavoidably contains two chemically different blocks. From polymer solution theory, we know that two chemically different polymers have the tendency to demix above some critical concentration. Thus, we may expect microphase segregation in the micellar corona.

Segregation in micellar coronas was observed experimentally in micelles with a cross-linked core[9,10] and complex coacervate core micelles.[11,12] The micelles reported in refs 9–11 feature a laterally segregated two-compartment corona. Micelles of this type are usually referred to as Janus micelles. The micelles with a cross-linked core were shown to act as supersurfactants and experience higher levels of self-assembly.[9,10]

Below, we will use a self-consistent field (SCF) approach to study the structural as well as thermodynamical properties of micelles formed by $A_NB_MC_N$ triblock terpolymers. We consider highly symmetrical terpolymers with an insoluble middle block *B* and two equally soluble side blocks *A* and *C*. The length of the corona blocks *N* is chosen to be long enough to be in the spherical micellar regime.[13] In the SCF method, the interactions between the monomers are accounted for using Flory−Huggins dimensionless exchange interaction parameters.[14] The value of this parameter is negative for attraction and positive for repulsion. The triblock terpolymer $A_NB_MC_N$ is equivalent to the copolymer $A_NB_MA_N$ if the monomers *A* and *C* have a zero interaction parameter with each other ($\chi_{AC} = 0$) and equal interaction parameters with the other monomers ($\chi_{AS} = \chi_{CS}$, $\chi_{AB} = \chi_{BC}$). Therefore, in the limit of low χ_{AC}, the thermodynamic and structural properties of terpolymer micelles are similar to those of copolymer ones. However, above some critical value of χ_{AC}, we expect a transition to Janus type micelles with various novel characteristics.

The theory indicates that in the corona of spherical micelles one can distinguish at least three distinct regions.[15,16] The inner region, that is closest to the core, is characterized by a power law density decay (depending on the solvent quality) which is forbidden for the free chain ends (best seen when the micelle resembles a star, i.e., for a small core). Further away from the

† Wageningen University.
‡ Institute of Macromolecular Compounds, Russian Academy of Sciences.
§ Institut Pluridisciplinaire de Recherche sur l'Environnement et les Matériaux.

10.1021/ma800130q CCC: $40.75
Published on Web 04/30/2008

core, the curvature of the micelle is less pronounced; that is, the local curvature is quasi-planar and as a consequence the density profile is parabolic-like. Finally, at the periphery, the profile decays exponentially toward the bulk. The same regions must exist in micelles with a segregated corona.

Also relevant for Janus micelles, we know that macrophase segregation of polymers in bulk solutions depends on interaction parameters, polymer concentrations, chain lengths, and so forth.[14] One of the issues is which known results of the bulk phase behavior are transferable to the present problem. For example, the critical condition for segregation of two polymers *A* and *C* of equal length *N* and total volume fraction φ_p in a nonselective good solvent is given by $N\varphi_p\chi_{AC} = 2$.[14,17] Due to the dependence of the polymer volume fraction in the corona on the distance from the core, it is not *a priori* known how and when segregation will occur. Also, from macroscopic phase studies, we know that the interface between two phases diverges upon the approach of the critical point.[18] For Janus micelles, however, we expect a nontrivial structure of the interface between *A* and *C* and it is clear that the width of the interface cannot exceed the size of the micelle. Indeed, the characterization of the interface in the corona is one of the main issues of this paper. At this stage, we may anticipate various other consequences of having an interface between *A* and *C*. One of these is that the spherical topology of the micelle not necessarily is found even when the length of the *A* and *C* blocks are sufficiently large.

In the most naive model, the micellization is a first-order phase transition. In this picture, the micelle size is constant. Upon an increase in the overall polymer concentration above the critical micelle concentration (cmc), only the number of micelles increases. This occurs in the naive model at a fixed polymer chemical potential. However, as the size of the micelles remains finite, it must be the case that the micellization transition is smooth, that is, it cannot be first-order. The fundamental issue here is that each micelle has translational degrees of freedom and the mixing entropy on the micellar level depends on the micelle concentration. In the surfactant science community, this fact is well-recognized.[19] It is well-known that upon increasing the overall surfactant concentration the micelle concentration increases sharply (in line with the naive model). The free surfactant (unimer) concentration, however, does not remain constant but increases slightly. This increase of the unimer concentration has corresponding effects on the micelle size. Indeed, with increasing micelle concentration, the micelle size increases necessarily. In many cases, this increase in aggregation number is, above some threshold concentration, accompanied by a change in micellar geometry.[20] This point is often referred to as the second cmc and also occurs as a cooperative but smooth transition.[21,22]

For simple diblock copolymer micelles, there exists scaling predictions for many of their properties such as the aggregation number, the size of the core and corona, and so forth as a function of the block lengths.[13] For these predictions, typically the translational degrees of freedom of the micelles is ignored; that is, these are made in the naive phase transition picture. The argument that is used to motivate this naive picture is that, with increasing size of the micelles, that is, with increasing aggregation number, the micellization transition gradually becomes closer to a true first-order transition. Below, we will keep the micellar translational entropy in our considerations.

The remainder of this paper is as follows. Before we can examine the structure of micelles in the SCF model, it is necessary to verify that the micelles that have been generated are thermodynamically stable. We therefore will start our theoretical section with a short review of the thermodynamics of small systems that is used for this. This is followed by a brief review of the SCF model. In the Results section, we will focus on the symmetrical case only, that is, $N_A = N_C$, for which the solvent is good and nonselective for the corona chains and poor for the core block. The conclusions are formulated at the end as usual.

Theory

Small System Thermodynamics. Self-consistent field theory for self-assembly rests on the notion of thermodynamics of small systems. The approach developed by Hill[23] assumes that the real system is divided into $\aleph$ subsystems, where each system has the same composition as the overall system. The Gibbs energy is then optimized with respect to the number of small systems. In the case of a micellar solution, each subsystem will contain one micelle and thus $\aleph$ is identified as the number of micelles.[19] A combination of the first and second laws of thermodynamics gives for the differential of the Gibbs energy of the macroscopic system

$$dF = -S\,dT + V\,dP + \sum_i \mu_i\,dn_i + \epsilon\,d\aleph \tag{1}$$

where the value conjugated to the number of small systems is the subdivision work. All other quantities have their usual meaning. The subdivision work is also the work necessary to create one more micelle in the system with a fixed number of molecules n_i of each type i; therefore, it can be alternatively identified as the aggregation work. For an incompressible system with a fixed number of molecules and temperature T, the minimum of the Gibbs energy is defined by

$$\frac{\partial F}{\partial \aleph}_{T,P,n_i} = \epsilon = 0 \tag{2}$$

$$\frac{\partial \epsilon}{\partial \aleph}_{T,P,n_i} > 0 \tag{3}$$

Note that the aggregation work ϵ is related to the overall grand potential in the system, that is, $\epsilon\aleph = F - \Sigma_i\, n_i\mu_i$. Indeed, for homogeneous bulk systems, this quantity is necessarily zero.

Even though we have introduced just one number, $\aleph$, of the total number of micelles in the system, this does not imply that it is assumed that all micelles are identical. In fact, the result thus far is completely general and allows for any micelle size distribution, as well as for the case that micelles strongly interact. As usual, however, classical thermodynamics cannot provide us with much more molecular insight. For this, we must turn to a molecular model. Within such model, we have to make approximations. Even though micelles are not uniform in real life, our model will consider the so-called most-probable micelle. This is reasonable because the size distribution (of spherical micelles) is usually sharp. Of course, there will always be a distribution in sizes and, sometimes, shapes. Fluctuations in micelle size and shape can be estimated from the theoretical model, but this usually involves approximations as well.

Realizing that ϵ is the conjugate variable coupled to the number of micelles $\aleph$, we can also identify ϵ as an excess chemical potential of the micelle. From this perspective, it is natural to write for dilute micellar solutions

$$\epsilon = \ln \varphi_m + \epsilon_m \tag{4}$$

Here, as well as in the remainder of this paper, we have omitted the thermal energy k_BT factors. This means that all energy units are expressed in units of k_BT. In eq 4, φ_m is the volume fraction of micelles, and thus, the first term on the right-hand side gives the entropic contribution that accounts for the translational degree of freedom of the micelle. ϵ_m may then be identified as the (dimensionless) translationally restricted grand potential of

the micelle. As we will see, the latter quantity is the primary thermodynamic quantity in the SCF analysis.

Self-Consistent Field Modeling. In the previous paragraph, we presented generally applicable thermodynamic considerations for self-assembling systems. In a molecular model, there are always details and approximations such that the application of these general considerations is delicate. We will therefore first go into details about the thermodynamic aspects from the perspective of the SCF modeling. Only after that we will outline the machinery of the SCF method. From here on, all lengths are made dimensionless with the segment length l.

Thermodynamics of Self-Assembly for the SCF Approach. The first issue is that we need to solve the SCF equations (to be specified below) numerically. To do this, we need to introduce a discretization scheme. We will use the method of Scheutjens and Fleer for this.[24,29] According to this method, there is a system of lattice coordinates in which layers are identified over which the mean-field approximation (to be specified below) is implemented. Effectively, this implies that one can find only those micellar geometries that are consistent with the chosen geometry. In addition, it appears that the micelles that are predicted in this method have no collective degree of freedom. Usually, one considers just a single micelle in the (small) system, and effectively one thus focuses on so-called most likely micelles. One advantage of a lattice model is that the volume of the molecules is quite naturally accounted for, as each monomer or each segment of the chain occupies a single lattice site. This is usually combined with an incompressibility condition which effectively says that the volume is fully occupied by molecular species. In such an approach, there is no volume work in the thermodynamic description, and therefore, we can write for the Gibbs energy (which in the incompressible limit equals the Helmholtz energy) of a small system F as it appears in the SCF model

$$F = \sum_i n_i \mu_i + \epsilon_m \tag{5}$$

Introducing excess quantities by subtracting all bulk quantities, that is, $F = F^\sigma + Vf^b$, where V is the volume of the small system and f^b if the free energy density in the bulk, we obtain

$$F^\sigma = \sum_j n_j^\sigma \mu_i + \epsilon_m \tag{6}$$

Below, we will show that from optimizing the canonical partition function the F value is available and eq 5 is then used to compute ϵ_m. The differential of the translationally restricted grand potential is given by

$$d\epsilon_m = -s\, dT - \sum_j n_j^\sigma\, d\mu_j \tag{7}$$

where the summation over j is over all nonsolvent components. Below, we will have only one polymeric component (p) and use it for the aggregation number $g \equiv n_p^\sigma$. The Gibbs−Duhem equation for this case is, for fixed temperature, given by

$$\frac{\partial \epsilon_m}{\partial \mu_p} = -g \tag{8}$$

From the modeling, we obtain information on the aggregation number dependence of the translationally restricted grand potential $\epsilon_m(g)$, as well as that for the chemical potential $\mu_p(g)$. From eq 8, we can find

$$-\frac{\partial g}{\partial \epsilon_m} = \frac{1}{g}\frac{\partial g}{\partial \mu_p} = \frac{\sigma_g^2}{g} \tag{9}$$

where $\sigma_g^2 = \langle g^2 \rangle - \langle g \rangle^2$ is a measure for the fluctuation in the aggregation number of the micelles. As this number is necessarily positive, we conclude that for stability $\epsilon_m(g)$ is a decreasing function with g or equivalently $\mu_p(g)$ is an increasing function of g. At this point, it is illustrative to make a link to the classical thermodynamics. It is quite natural to expect that the average aggregation number is a decreasing function of the number of micelles in the system and thus that $\partial \aleph / \partial g < 0$. The stability in the small system $\partial \epsilon_m / \partial g < 0$ is thus closely related to that in the overall system $\partial \epsilon / \partial \aleph > 0$.

At this point, it is necessary to understand that in the SCF calculation the total volume available for a micelle is not influencing the calculations (as long as this volume is sufficiently large such the micelle does not interact with its neighbors). The simple reason for this is that the micelle is effectively fixed with its center of mass to a point in the coordinate system. For example, in a spherical coordinate system, the micelle is fixed in the center. We may use eq 4 to estimate the actual volume available for a given micelle with a known aggregation number g. This equation implies $\varphi_m = e^{-\epsilon_m}(g)$ (recall that ϵ_m is made dimensionless by the thermal energy $k_B T$). Assuming that a micelle is composed of a dense packing of chains, the volume fraction of micelles may be approximated by $\varphi_m \approx \upsilon g N / V_{ss}$, where υ is a unit volume occupied by a segment. Using this, we can compute the overall volume fraction of polymer chains

$$\varphi_p^t = \varphi_p^b + \varphi_m = \varphi_p^b + e^{-\epsilon_m} \tag{10}$$

Using this, we can distinguish two regimes. Below the cmc, we will have $\varphi_m \ll \varphi_p^b$ and $\varphi_p^t \approx \varphi_p^b$, whereas above the cmc we will have $\varphi_m > \varphi^b$ and $\varphi_p^t \approx \varphi_m$. From this, it is easy to see that φ_m is limited to unity or, equivalently, $\epsilon_m > 0$. Indeed, for small values of ϵ_m, one should account for the interaction between micelles. This condition requires special attention. We will consider dilute micellar systems only.

The Machinery of SCF Modeling. At the basis of the SCF theory is the free energy which is a functional of the volume fraction profiles $\varphi(r)$ and so-called self-consistent potential profiles $u(r)$. As mentioned above, this free energy is optimized numerically. We follow Scheutjens and Fleer[24] who suggest to use one characteristic length l both to discretize the space and to segmentize the chains. The discretization of space leads to lattices in which layers of sites are identified. We will refer to each layer by a coordinate r. Typically, we can consider several lattice geometries. Spherical micelles can be modeled using a spherical geometry. In this case, $r \equiv r = 1, ..., M_r$ are lattice layers with an increasing number of lattice sites $L(r) \propto r^2$. Long cylindrical micelles can also be modeled using a single coordinate, that is, when end effects are ignored. In this case, the number of lattice sites per unit length of the cylinder obeys $L(r) \propto r$. Bilayers are flat association colloids, and for this system we use $r \equiv z = 0, ..., M_z$. Again, using one single coordinate implies that boundary effects are ignored. Now, the number of lattice sites in layer z is constant; that is, per unit area it is $L(z) = 1$ for all z. In these three-coordinate systems, we have just a single coordinate and we will refer to these systems as the one-gradient version of the SCF model. Typically, we have reflecting boundary conditions at the system boundaries.

Below, we will also use a two-gradient version in which the coordinate $r = (r, z)$, where $r = 1, ..., M_r$ are concentric rings of lattice sites in which the number of lattice sites $L(r) \propto r$ and $z = 1, ..., M_z$ are flat lattice layers along the long axis of the cylinder.[25−27] We have reflecting (mirror-like) boundary conditions at all lattice boundaries.

For the general case, we can write the (dimensionless) free energy of the systems in terms of two conjugated quantities, namely, the segment volume fractions $\varphi(r)$ and the segment self-consistent potentials $u(r)$

$$F = -\ln Q[u] - \sum_{\mathbf{r}} L(\mathbf{r}) \sum_{x} u_x(\mathbf{r})\, \varphi_x(\mathbf{r}) + F^{\text{int}}[\varphi] + \sum_{\mathbf{r}} u'(\mathbf{r})\, L(\mathbf{r}) \left(\sum_{x} \varphi_x(\mathbf{r}) - 1 \right) \quad (11)$$

with

$$F^{\text{int}} = \frac{1}{2} \sum_{\mathbf{r}} L(\mathbf{r}) \sum_{x,y} \varphi_x(\mathbf{r})\, \chi_{xy} \langle \varphi_y(\mathbf{r}) - \varphi_y^{\text{b}} \rangle \quad (12)$$

In eqs 11 and 12, the indices x and y run over all segment types (i.e., A, B, C, S), and χ expresses, as in the Flory−Huggins theory, the strength of the nearest-neighbor interactions. φ^{b} refers to the volume fraction in bulk defined as the region of space far from the micelle. The site average, indicated by the angular brackets, accounts for local and nonlocal contributions to the interaction energy and is computed by $\langle X(r) \rangle = \Sigma'_{\mathbf{r}'} \lambda_{\mathbf{r}'\text{-}\mathbf{r}}(\mathbf{r})\, X(\mathbf{r}') \approx X(\mathbf{r}) + \lambda \nabla^2 X(\mathbf{r})$, where the prime on the sum sign indicates that the sum is over all neighboring sites of $\mathbf{r}$. The *a priori* step probabilities λ are geometry dependent and obey the detailed balance $L(\mathbf{r}')\ \lambda_{\mathbf{r}\text{-}\mathbf{r}'}(\mathbf{r}') = L(\mathbf{r})\ \lambda_{\mathbf{r}'\text{-}\mathbf{r}}(\mathbf{r})$. Moreover, they are normalized $\Sigma'_{\mathbf{r}'} \lambda_{\mathbf{r}'\text{-}\mathbf{r}}(\mathbf{r}) = 1$. The fourth term in eq 11 decouples the volume fractions of the components, where the Lagrange parameter $u'(r)$ is linked to the incompressibility constraint (sum over all volume fractions equals unity). The first term of eq 11 features the partition function for the (u, V, T) ensemble $Q = \Pi_i \{ (q_i([u_i]))^{n_i}/n_i! \}$, where i represents the type of molecule, that is, the solvent, polymer, and so forth. Finally, the second term in eq 11 is a Legendre transformation such that the first two terms essentially give the dimensionless entropy.

The optimization of the free energy leads to the equations

$$\frac{\partial F}{\partial \varphi_x(\mathbf{r})} = -u_x(\mathbf{r}) + u'(\mathbf{r}) + \sum_{y} \chi_{xy} \langle \varphi_y(\mathbf{r}) - \varphi_y^{\text{b}} \rangle = 0 \quad (13)$$

$$\frac{\partial F}{\partial u_x(\mathbf{r})} = -\frac{\partial \ln Q}{\partial u_x(\mathbf{r})} - L(\mathbf{r})\, \varphi_x(\mathbf{r}) = 0 \quad (14)$$

$$\frac{\partial F}{\partial u'(\mathbf{r})} = L(\mathbf{r}) \left(\sum_{x} \varphi_x(\mathbf{r}) - 1 \right) = 0 \quad (15)$$

These equations form the basis of the SCF machinery. Equation 13 specifies how the segment potentials follow from the volume fractions. Equation 14 gives a method to compute the volume fraction from the potentials. Below, we present a more practical alternative (but equivalent) route. Equation 15 gives the compressibility constraint.

An efficient route to compute the partition function starts with the Boltzmann weights $G_x(\mathbf{r}) = \exp(-u_x(\mathbf{r}))$, which are generalized to a segment ranking number dependent quantity $G_i(\mathbf{r}, s) = \Sigma_x\, G_x(\mathbf{r})\, \delta_{i,s}{}^{x}$, where $\delta_{i,s}{}^{x} = 1$ when segment s of molecule i is of segment type x and zero otherwise. These Boltzmann weights are used in the propagator equations, which are the discrete versions of the Edwards equation:[28]

$$G_i(\mathbf{r}, s|1) = G_i(\mathbf{r}, s)\, \langle G_i(\mathbf{r}, s-1|1) \rangle \quad (16)$$

$$G_i(\mathbf{r}, s|N) = G_i(\mathbf{r}, s)\, \langle G_i(\mathbf{r}, s+1|N) \rangle \quad (17)$$

for $s = 1, N_i$ (in our case, the block copolymer has $N = N_A + N_B + N_C$ segments), where the angular brackets again indicate a geometry dependent site averaging. The propagators are started with $G_i(\mathbf{r}, 1|1) = G_i(\mathbf{r}, 1)$ and $G_i(\mathbf{r}, N|N) = G_i(\mathbf{r}, N)$, $\forall \mathbf{r}$ and produce $q_i = \Sigma_{\mathbf{r}}\, L(\mathbf{r})\, G_i(\mathbf{r}, N|1)$. Now, eq 14 may be used to evaluate the volume fraction profiles. An efficient implementation of this is by the use of the so-called composition law which combines two subpartition functions:

$$\varphi_i(\mathbf{r}) = \frac{n_i}{q_i} \sum_{s=1}^{N_i} \frac{G_i(\mathbf{r}, s|1)\, G_i(\mathbf{r}, s|N)}{G_i(\mathbf{r}, s)} \quad (18)$$

The volume fraction of the solvent in the bulk as an input parameter and eq 18 applied for the solvent gives $\varphi_S(\mathbf{r}) = \varphi_S^{\text{b}}$ $G_S(\mathbf{r})$. Note that in a two-component system $\varphi_S^{\text{b}} = 1 - \varphi_{\text{p}}^{\text{b}}$, where $\varphi_{\text{p}}^{\text{b}} = n_{\text{p}} N_{\text{p}}/q_{\text{p}}$.

Table 1. List of All Default Flory−Huggins Interaction Parameters[a]

χ	S	A	B	C
S	0	0	2	0
A	0	0	2	0
B	2	2	0	2
C	0	0	2	0

[a] The default block copolymer is $A_{100}B_{70}A_{100}$. The monomeric solvent is S, and in some of the calculations one A block is replaced by a block of C segments with equal length as the A block.

The equations are solved numerically up to high precision.[29] For the self-consistent solution, it is possible to evaluate the grand potential $\epsilon_{\text{m}} = \Sigma_{\mathbf{r}}\, L(\mathbf{r})\, \omega(\mathbf{r})$, where the dimensionless grand potential density $\omega(\mathbf{r})$ is

$$\omega(\mathbf{r}) = -\sum_{x} \phi_x(\mathbf{r}) u_x(\mathbf{r}) - \sum_{i} \frac{\phi_i(\mathbf{r}) - \phi_i^b}{N_i} + \frac{1}{2} \sum_{x,y} \chi_{xy} \{ \phi_x(\mathbf{r}) (\langle \phi_y(\mathbf{r}) \rangle - \phi_y^b) - \phi_y^b (\phi_y(\mathbf{r}) - \phi_y^b) \} \quad (19)$$

The chemical potential of the components can be expressed in terms of the bulk volume fractions, as the bulk is in full equilibrium with the micellar objects:

$$\mu_i - \mu_i^{\#} = \ln \varphi_i^{\text{b}} + 1 - N_i \sum_{j} \frac{\varphi_j^{\text{b}}}{N_j} - \frac{N_i}{2} \sum_{x,y} (\varphi_x^{\text{b}} - \varphi_{Ai}^{*}) \chi_{AB} (\varphi_B^{\text{b}} - \varphi_{Bi}^{*}) \quad (20)$$

where $\varphi_{Ai}{}^{*} = \Sigma_{s=1}{}^{N_i}\, \delta_{i,s}{}^{A}/N_i$ is the fraction of A segments in molecule i and $\mu_i^{\#}$ is the chemical potential of molecule i in the reference phase (which is a phase composed of purely molecules of type i).

Results

***ABA* Micelles.** In this section, we employ the one-gradient version of the SCF method on a spherical lattice to collect properties of $A_N B_M A_N$ polymer micelles. In this geometry, all properties of the system depend only on the distance r from the center of the coordinate system. All values within concentric spherical layers are averaged implementing the mean-field approximation along the angular coordinates. Hence, spherical symmetry is imposed on the system. We use local volume fractions of components to characterize the structural properties of the micelle.

To reduce the number of variables involved, we fix the parameters related to the micellar core and vary only those related to the corona. The Flory−Huggins interaction parameter between B and the solvent S, χ_{BS}, is 2, and the length of the solvophobic block (M) is 70 segments. The interaction parameter between the different segments in the copolymer χ_{AB} is also set to 2. This parameter is very important for the ordering in polymer melts, where it drives the self-organization. In our case, it mainly defines the sharpness of the interface between the core and corona segments in the micelle. In the dilute polymer system, micellization is governed by the polymer−solvent interactions. The insolubility of the middle block drives the aggregation, whereas crowding and repulsion of the chains in the solvated micellar corona provide the stopping force. The efficiency of the stopping mechanism is strongly affected by the length N of the corona blocks and the interaction parameter χ_{AS}. Unless specified otherwise, the corona block consists of $N_A = 100$ segments and $\chi_{AS} = 0$. We summarize the set of "default" parameters in Table 1.

Before we turn to the structural properties of spherical $A_{100}B_{70}A_{100}$ micelles, let us first discuss their stability from the

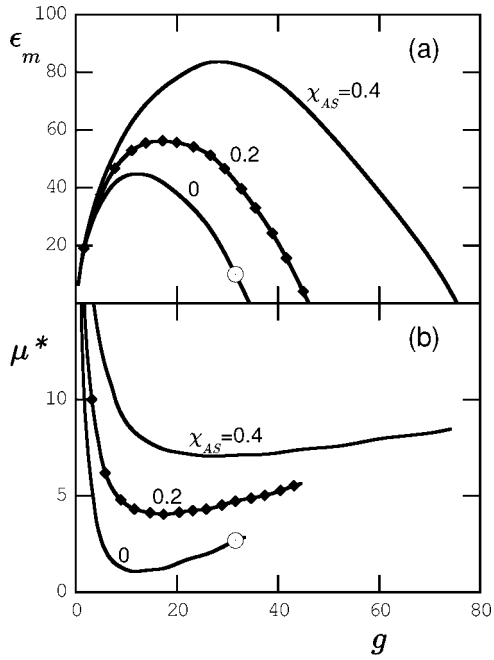

Figure 1. Translationally restricted grand potential ϵ_m of the $A_{100}B_{70}A_{100}$ micelle (a) and copolymer chemical potential, where $\mu^* = \mu_p - \Delta\mu$ (b), versus aggregation number g for $\chi_{AS} = 0$, 0.2, and 0.4. With the tilted square symbols, we show ϵ_m and μ_p for $A_{100}B_{70}C_{100}$ terpolymer micelle with $\chi_{AS} = \chi_{CS} = 0.4$ and $\chi_{AC} = 0.8$. Note that due to repulsion in the two-component corona the tilted squares go on top of the curves for copolymeric micelles with $\chi_{AS} = 0.2$. For presentation purposes, the chemical potential values are shifted by the constant values $\Delta\mu_{\chi_{AS}}$ with $\Delta\mu_0 = 278$, $\Delta\mu_{0.2} = 244$, $\Delta\mu_{0.4} = 211$, and $\Delta\mu = 234$ for the $A_{100}B_{70}C_{100}$ micelle. The point corresponding to the profile in Figure 2 is indicated with an open circle.

viewpoint of thermodynamics of small systems. In Figure 1, we plot the translationally restricted grand potentials (Figure 1a) of the micelles and the chemical potentials of the terpolymers (Figure 1b) as a function of aggregation number g for a selected set of χ_{AS} values. The criterion for thermodynamic stability is defined by eqs 2 and 3. At low aggregation numbers, the translationally restricted grand potential first grows. This means that micelles with an aggregation number less than a certain threshold value are unstable. The smallest thermodynamically stable micelle appears at the maximum of the $\epsilon_m(g)$ curve, which coincides with the minimum of the chemical potential (cf. Figure 1b). For example, in the case of our "default" system with athermal corona blocks ($\chi_{AS} = 0$), only micelles with $g > 12$ are stable. Using eq 10, one can estimate both the cmc and the overall polymer volume fraction corresponding to the smallest stable micelle. The cmc for micelles with athermal corona chains turns out to be as low as $\varphi = 10^{-18}$, which is well below experimental resolution. The cmc's for less soluble corona chains are even lower. In other words, we expect the chosen triblocks to form micelles at all practical polymer concentrations.

One of the approximations implied in our model is that micelles do not interact with each other. This assumption does not hold at high polymer concentrations. Thus, the results of the present SCF modeling are inaccurate when the micelles start to overlap. Below, we will select typical conditions, defined as those systems for which the translationally restricted grand potential $\epsilon_m = 10$. The range of deviations from the chosen typical conditions that are still experimentally relevant is quite narrow due to the exponential dependence of the polymer volume fraction φ_p on the grand potential ϵ_m (cf. eq 10). A rough evaluation shows that our estimate for the entropy of the micelles becomes inaccurate for micelles with $\epsilon_m = 5$, meaning that for these micelles the micellar interactions should be

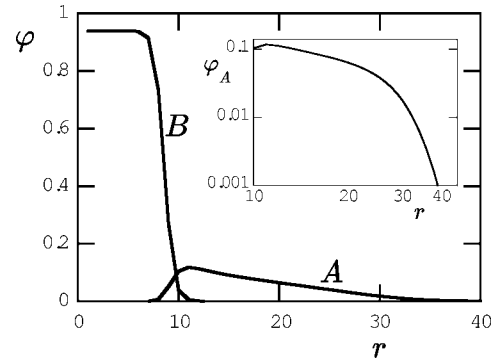

Figure 2. Radial volume fraction profiles of the A and B components in a spherical micelle composed of $A_{100}B_{70}A_{100}$ copolymers. Inset: corona profile, log−log scale.

accounted for. On the other hand, micelles with a translationally restricted grand potential $\epsilon_m = 25$ are the most probable ones at an overall volume fraction of polymer $\varphi_m \approx 10^{-11}$. Concentrations as low as this are irrelevant for any experimental technique. Thus, the relevant aggregation numbers are in the range $g \in [28, 33]$.

For our "default" system (shown with an open circle in Figure 1a), $\epsilon_m = 10$ translates to an overall polymer volume fraction $\varphi_t \approx 4.5 \times 10^{-5}$ and a typical distance between two micelles of $\approx 570l$. The aggregation number of the most probable micelle at this polymer concentration is $g \approx 32$. In Figure 2, we show the radial volume fraction profile of both the core A and the corona B monomers in this most likely micelle. The micelle consist of a dense core and a solvated corona. The polymer fraction in the core φ_B is constant. Assuming that it depends only on the solubility and the length of the middle block B, we should expect the same volume fraction as that of a corresponding collapsed homopolymer in a poor solvent. Indeed, the polymer fraction estimation based on the mean-field type free energy density

$$F = (1 - \varphi_B)\ln(1 - \varphi_B) + \chi_{BS}\,\varphi_B(1 - \varphi_B) \qquad (21)$$

and vanishing osmotic pressure

$$\pi = F - \varphi_B\frac{\partial F}{\partial \varphi_B} = \varphi_B + \ln(1 - \varphi_B) + \chi_{BS}\varphi_B^2 = 0 \qquad (22)$$

yields in $\varphi_B = 0.93$, which fits the SCF results for the polymer fraction in the core very well. In the expression for free energy, eq 21, we neglected the entropy of the collapsed polymer and used the incompressibility condition eq 15.

The micellar corona is formed by the A segments immersed in a good solvent. The polymer volume fraction in the corona monotonously decreases from the core surface to the exterior of the micelle. Because of the crowding near the core, the chains in the micellar corona are stretched as compared to the case of free polymers. The model by Daoud and Cotton[30] predicts that the polymer density φ_A is proportional to $r^{-4/3}$. In Figure 2, we present the density profile of the corona in log−log coordinates. In line with the Daoud−Cotton result, the region $12 < r < 25$ is approximately a straight line with a slope close to $-4/3$.

Although the SCF modeling is targeted to a single micelle, the thermodynamic properties of the small system apply to the whole system. We demonstrated this by estimating the volume fraction of micelles using ϵ_m. Next, according to eq 9, the steepness of the $\epsilon_m(g)$ curve of Figure 1a is inversely proportional to the relative fluctuation of the aggregation number. Thus, one can estimate the micellar size distribution at a given chemical potential. Note that in the SCF model the fluctuations diverge as in a first-order phase transition at the point were the first thermodynamically stable micelles appear. The first ap-

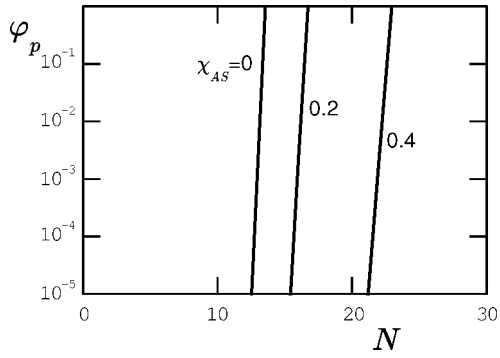

Figure 3. Sphere-to-rod transition for $A_NB_{70}A_N$ copolymer micelles as a function of the corona block length and bulk polymer fraction for $\chi_{AS} = 0$, 0.2, and 0.4. Copolymer compositions to the right from the indicated lines correspond to spherical micelles.

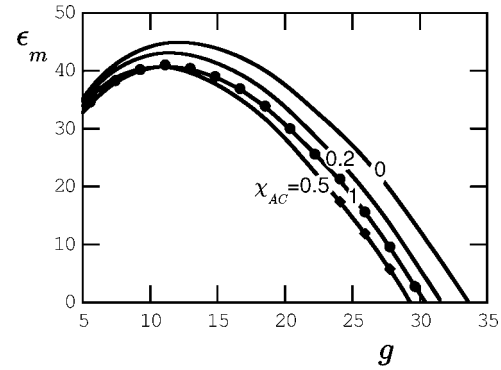

Figure 4. Translationally restricted grand potentials ϵ_m of $A_{100}B_{70}C_{100}$ micelles with $\chi_{AC} = 1$, 0.5, 0.2, and 0. Parts of the curves corresponding to micelles with segregated coronas are marked with circles. The horizontal dashed line at $\epsilon_m = 10$ points to the "typical micelle" condition.

pearance of micelles occurs as a jump from a zero micelle concentration to a finite albeit very small value. In this respect, the SCF model is wrong: we know that the micellization transition is smooth. We note however that the error is not severe, as the concentration of micelles is exponentially small. Nevertheless, we should be aware of this when micellar properties are considered near this maximum.

One potentially unsafe assumption we made thus far is the choice of a spherical lattice. It is well-known that block copolymers are potentially able to form cylindrical or lamellar structures. While for short surfactants the preference for one geometry over the other depends on the overall surfactant concentration, for polymeric micelles it is mostly defined by the molecular composition. We now explicitly justify our choice of the spherical geometry for the present triblocks. In Figure 3, we present the diagram of states in the region of the sphere-to-rod transition as a function of the length N of the soluble block for $\chi_{AS} = 0$, 0.2, and 0.4. We obtained this diagram of states by comparing the chemical potentials of unimers in equilibrium with micelles with a spherical or a cylindrical geometry. In a narrow compositional range, where both cylindrical and spherical micelles are thermodynamically stable, that is, eqs 2 and 3 are satisfied, the structure corresponding to the lowest chemical potential dominates. Exactly at the transition point, the chemical potentials of unimers in equilibrium with spherical and cylindrical micelles are equal. In the coexistence region the balance between the two may be shifted by changing the overall polymer concentration. One can note that for micelles with an athermal corona the sphere-to-rod transition occurs around $N \approx 13$. The transition from cylindrical micelles to lamellae (not shown) occurs for triblocks with even shorter soluble blocks. Our default $N = 100$ is much larger, and thus, our analysis of spherical micelles is sufficient.

The two-gradient version of the SCF method on a cylindrical lattice that we use in the next section imposes only the axial symmetry on the system. Therefore, among others, it allows for the formation of spherical, rodlike, and lamelar structures. In this way, there is no need for an explicit check of the preferred geometry, as the most probable shape of the aggregate will be chosen automatically by the SCF machinery. Nevertheless, the preliminary analysis we made above is still useful, because the energy barriers between different micelle geometries may sometimes prevent the SCF from finding the best solution.[27] Hence, it is important to know that $A_{100}B_{70}A_{100}$ polymer micelles are spherical.

***ABC* Micelles.** In this section, we present results of SCF modeling of $A_{100}B_{70}C_{100}$ micelles. The only difference between this and our "default" system from the previous section is that here we introduce a repulsion between the two soluble blocks A and C. The repulsion between the components has the potential to drive the A and C segments to separate regions in the corona. Micelles with a laterally segregated corona do not have a spherical symmetry; therefore, we need to use a two-gradient version of the SCF method on a cylindrical lattice. In this geometry, all profiles depend only on the axial coordinate z and the distance from the axis of cylindrical coordinate system r. All properties are averaged along the angular coordinate.

In Figure 4, we present the grand potential ϵ_m of micelles with different segregation factors between blocks A and C. This plot provides the basis for the analysis of the thermodynamic stability of the micelles. In fact, the way to analyze it is the same as above in Figure 1a. As a reference, we plot ϵ_m for triblocks with no repulsion between the soluble blocks ($\chi_{AC} = 0$). The same curve is plotted in Figure 1a for $\chi_{AS} = 0$. The effect of the repulsion between the corona components has only a minor influence on the $\epsilon_m(g)$ dependence. Hence, the aggregation numbers, the cmc's, and the stability regions are close to those of *ABA* micelles. At the overall polymer fraction $\varphi_t \approx 4.5 \times 10^{-5}$, which, as before, translates to $\epsilon_m = 10$, the aggregation numbers range from 26 to 32 depending on the value of χ_{AC}.

Below a critical value of the segregation factor χ_{AC}^{crit}, the corona of the micelle remains mixed. In the special symmetrical case we consider, this means that at any spot in the corona equal fractions of A and B are found. The high symmetry of the triblocks makes it possible to include the segregation factor as a correction to the solvent quality for corona blocks. As shown in the Appendix, in the mean-field approximation, the segregation factor enters all analytical expressions for the corona as a part of an effective solvent quality parameter $\chi_{Seff} = \chi_S - (1/4)\chi_{AC}$. This substitution suggests that the overall polymer density profile and the aggregation numbers of $A_NB_MC_N$ micelles will be the same as these properties of an $A_N{}^*B_MA_N{}^*$ micelle where A^* is identical to A except for the solvent quality which is given by χ_S^{eff}. In Figure 1, we plot the grand potential of an $A_{100}B_{70}C_{100}$ micelle as a function of aggregation number. Although $\chi_{AS} = \chi_{CS} = 0.4$, $\epsilon_m(g)$ goes on top of a curve corresponding to an $A_{100}B_{70}A_{100}$ micelle with $\chi_{AS} = 0.2$. This is due to the repulsion between the corona components ($\chi_{AC} = 0.8$), which is equivalent to the decrease of the Flory−Huggins parameter for a single component corona from $\chi_{AS} = 0.4$ to 0.2. This result was obtained using a spherical lattice; hence, the segregation was hindered by geometrical constraints.

In the two-gradient version of the SCF calculations, increasing the χ_{AC} value to above the critical value results in the segregation of the corona chains into two domains, with one rich in A and the other reach in C. The segregation restricts unfavorable

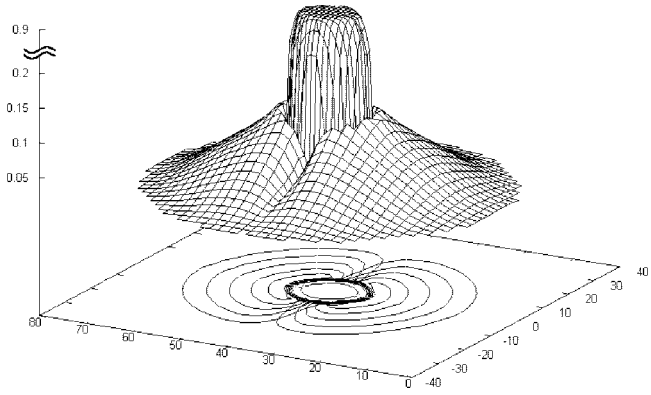

Figure 5. Volume fraction profile of a Janus micelle in a cylindrical coordinate system. The cross section through the center of the micelle is given. $\chi_{AC} = 1$.

contacts between the components to an interface between the domains. In the general case when the *A* and *C* blocks have a different affinity with the solvent or with the core or have different lengths, the domains are not necessarily equal and even core−shell corona structures may appear. For the highly symmetrical copolymer considered here, the lateral segregation into two equal hemispheres is the most favorable option. We show in Figure 5 an example of the structure of a micelle with an inhomogeneous corona. In this graph, we present not only the equal volume fraction contour plots for the core and the two corona blocks, but also the corresponding two-gradient volume fraction profiles. The center of mass is (by definition) at the $R = 0$ axis (volume fractions for positive *R* are identical to those at negative *R*). The numbering of the layers in the *z*-direction is arbitrary. Clearly visible is the dense core and the more swollen corona. The interface in the corona splits the micelle exactly into two structurally identical halves. This is true because of the symmetrical choice of the parameters used. Micelles with a lateral segregated domain structure are usually referred to as Janus type in contrast to core−shell−corona (onion) type.

With the tilted squares in Figure 4, we show the regions corresponding to micelles with a segregated corona. The transition depends on the micellar aggregation number, and consequently it can be induced by a change in overall polymer concentration. For $\chi_{AC} = 1$, we find micelles with a segregated corona for all aggregation numbers. The contour plots in Figure 6 show the overall polymer volume fraction profiles (a) and the volume fraction profiles of the *A* and *C* components (b) at typical conditions ($\epsilon_m = 10$). The interface between the domains is sharp, and the fraction of minor components inside the domains is negligible. Due to the presence of an extra interface, the overall shape of the corona deviates from sphericity toward the prolate ellipsoidal shape. The $\chi_{AC} = 0.5$ micelles with a relatively low aggregation number have a mixed corona. At typical conditions ($\epsilon_m = 10$), the micelle transforms into the Janus type and the contour plots are shown in Figure 6c and d. As this system is close to its transition point, the interface between the domains is wide, and the contents of the minor component in the "wrong" phase is high. For example, the volume fraction of monomer *A* in the *C* rich phase near the core of the micelle, depicted in Figure 6c and d, is approximately $\varphi \approx 0.03$, which is a third of the overall polymer volume fraction at this spot, which is $\varphi \approx 0.1$. The overall polymer volume fraction profile indicates that this micelle is nearly spherical.

Interestingly, the lowest curve in Figure 4 corresponds to $\chi_{AC} = 0.5$. This means that at a fixed grand potential (i.e., a fixed overall polymer (micelle) concentration) the micelle with χ_{AC}

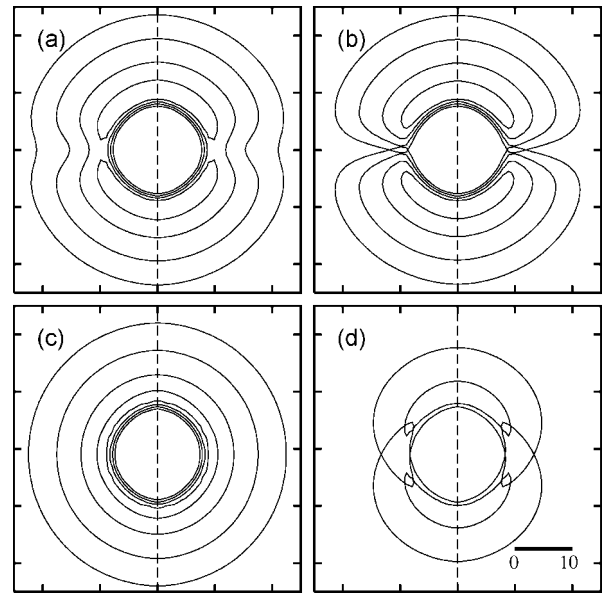

Figure 6. Polymer volume fraction profiles for Janus micelles with a segregated corona. The cross section through the symmetry axis is indicated. The overall volume fractions are shown in view graphs (a) and (c), and those of the *A* (solid line) and *C* (dashed line) components are presented in graphs (b) and (d).

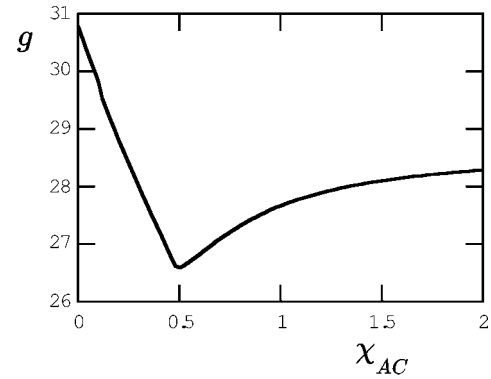

Figure 7. Aggregation number of $A_{100}B_{70}C_{100}$ micelles versus segregation factor χ_{AC}. The minimum corresponds to demixing transition.

$= 0.5$ is the smallest. From Figure 7, it is clear that the aggregation number as a function of the repulsion between the corona components $g(\chi_{AC})$ reverses its trend when the transition to the Janus type occurs. An imaginary experiment, in which one would be able to control the repulsion between the corona components without affecting other parameters, would show a non-monotonous dependence of the aggregation number with this χ_{AC} interaction parameter (cf. Figure 7). The minimum of the $g(\chi_{AC})$ plot corresponds to the demixing transition point.

Let us next turn our attention to the properties of the interface in the corona. Compared to the classical interface between segregated polymers in bulk solutions, in the Janus corona, there are several complications. As anticipated and shown in Figure 6, the polymer volume fraction is not constant along the *A*−*C* interface and the stretching of the chains depends on the distance from the core of the micelle. In Figure 8, we plot volume fraction profiles of the corona components near the core ($r = 12$) and in the periphery of the micelle ($r = 30$) in spherical coordinates, that is, $\theta = 0, ..., 180^\circ$. In this spherical coordinate system, connected to the center of the micelle, it is easy to see that the angle occupied by the interface only slightly depends on the distance from the core. This means that the interface widens toward the exterior of the micelle and that this dependence is close to linear. Unfavorable interactions between phase separated

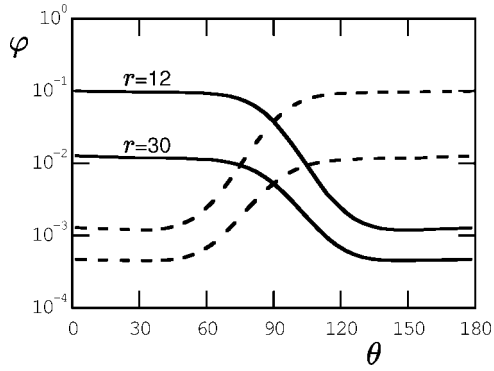

Figure 8. Angular distribution of volume fractions of monomers *A* (solid lines) and *C* (dashed lines) at distances $r = 12$ and $r = 30$ from the center of $A_{100}B_{70}C_{100}$ micelle. $\chi_{AC} = 1$.

polymers typically make the interface depleted by polymer and enriched by solvent as compared to the bulk phases.[31] This also holds for the intramicellar interface but only up to a certain distance from the core (not shown). This indicates that the contacts between the components *A* and *B* are rare in the outer part of the corona. The local volume fraction of the polymer is much lower than that necessary for macrophase segregation of the corresponding homopolymers in solution. Nevertheless, the interface persists due to the segregation in the inner part of the corona and the radial stretching of the chains. We will return to this in the Discussion.

Discussion

As long as there is no lateral segregation in the corona, the micellization of $A_{100}B_{70}C_{100}$ triblock terpolymers is similar to that of $A_{100}B_{70}A_{100}$ micelles. Any unfavorable interactions between unlike corona segments just result in a renormalization of the solvent quality of the corona segments. However, when the *A* and *C* segments repel each other sufficiently, the spherical symmetry is broken and Janus micelles form. As explained in the Introduction, the critical interaction parameter for the bulk system of two equally long polymers (A_N, C_N) in a common solvent *S* is given by $\chi_{AC}{}^{cr}N\varphi_p = 2$. This means that the onset of phase separation occurs at $\varphi_p^{cr} = 2/(N\chi_{AC})$. Translating this result to our problem indicates that as long as the volume fraction of polymer in the corona remains below φ_p^{cr}, the corona must remain laterally homogeneous. Inspection of our results shows that this is indeed the case. We only find laterally inhomogeneous coronas when, locally, the polymer volume fraction exceeds this value.

As discussed above, the highest concentration of corona segments is found just outside the core. We have checked for a number of cases where the onset of Janus micelle formation takes place when this highest volume fraction of corona segments just exceeds the critical value. The fact that at the regions further away from the core the volume fraction of polymer is below the critical value does not prevent the transition from occurring. Stating it differently, even though only part of the corona chains are subjected to demixing conditions, the full chain has to obey to the formation of the demixed state. The full analysis of this transition will be published elsewhere.

It is of interest to discuss the order of the transition as well. The demixing of polymers in segregated phases usually occurs as a first-order transition. However, when the binodal is crossed at the critical point, the transition is second-order. In our system, the critical volume fraction is at $\varphi_A^{cr} = \varphi_B^{cr} = 1/(N\chi_{AC})$. Due to the symmetry in our terpolymer, it is true that in the mixed corona $\varphi_A = \varphi_B$ at all coordinates. This means that (in this special case), the demixing can only be initiated by entering the two-phase region through the critical point. As a consequence, the transition cannot be first-order. This observation is consistent with the data presented in Figure 7, where the aggregation number shows a kink at the transition. This means that the second derivative of the free energy with respect to the chemical potential of the polymer is discontinuous, implying that the transition is second-order.

When we would have considered asymmetric terpolymers, we would have obtained an even more complicated system. Within the mean-field approximation, we might anticipate a first-order transition. However, due to the finite size of the micelle, the height of the free energy barrier in the demixing transition will remain finite and the Janus-micelle formation is at best first-order-like; that is, it can only approach this in the limit of infinitely long chains. This means that an ensemble of micelles will consist of micelles that continuously fluctuate from mixed to demixed coronas. Systemwise, this means that the transition is always smooth.

From macroscopic two-phase systems, we know that the width of the interface *W* diverges upon the approach of the critical point. In our system, the width of the interface cannot exceed the size of the micelle, and this fact probably will influence the onset of Janus-micelle formation slightly. Currently, we cannot estimate the importance of this effect.

The radial growth of the interfacial tension as shown in Figure 8 is of special interest as well. It was shown that the interface persists all the way to the dilute part of the corona volume fraction profile. In this region, the chains do not feel each other. It is noteworthy though that the local polymer concentration, at places where visually there is a clear interface, indeed can drop below the (bulk) critical value φ_p^{cr}. Only near the core does the polymer concentration exceed the critical value, and we believe that these higher polymer concentrations drive the formation of the interface. The high stretching of the chains in the radial direction (especially in the dead zone) helps to maintain the presence of the interface.

From macroscopic interfaces between polymer solutions, it is known that the interfacial tension γ is an increasing function of the segregation parameter χ_{AC}.[18,32] We therefore should expect that the excess free energy of the interface in the corona will be an increasing function of the interaction parameter. We found that this is the case (result not shown). However, from the above, it is obvious that the total amount of free energy present in the interface cannot be very high. From the grand potential density profiles $\omega(\mathbf{r})$, it is possible to estimate the excess free energy of the interface. Typically, we find values of the order of several k_BT per micelle. There are a number of important consequences of this. As there is so little free energy needed to create an interface, it must be possible to change the interface, that is, the shape and position. In other words, the interface should strongly fluctuate. In our SCF model, we cannot account for interface fluctuations, but they most likely will be large (especially near the critical conditions). We mention, however, that the present calculations were performed for relatively short chains and low aggregation numbers. In experimental cases, one may go to larger chains and higher aggregation numbers and then expect two-phase Janus micelles as the ground-state micelle.

To directly prove, in experimental situations, the existence of the Janus state of micelles is a major challenge.[33] In most cases, it will require labeling of the corona chains. This always has the potential effect of perturbing the structure. From Figure 6a, we see that there is a deviation from sphericity of both the core and the corona. Because of the high surface tension of the core−solvent interface, the core is almost spherical. Close inspection, however, shows that the core is an oblate ellipsoid. For micelles with a lower core−solvent interfacial tension, such

as complex coacervate core micelles,[11] the deformation of the core may be much more easily observable. The overall volume fraction profiles of the corona, however, indicate that the overall shape of the Janus micelle is a prolate ellipsoid. Such deviations from sphericity are the direct consequence of the interface in the corona and are the signature for Janus micelles. Finally, we have argued that in some cases the transition from mixed to demixed coronas can be triggered by increasing the aggregation number. For a given system, this may occur as a result of the increase in polymer (or micelle) concentration. Of course, for this to be operational, one needs to be sure that the aggregation is reversible, that is, that the core is not frozen in a glassy state. Again, complex coacervate core micelles may be the system of choice to observe this prediction.

Conclusions

Using a numerical self-consistent field approach, we studied the micellization of $A_NB_MC_N$ triblock terpolymers in a selective solvent. The *B* block forms a dense core and the two *A* and *C* blocks form a highly swollen corona. Using a cylindrical two-gradient coordinate system, we were able to study the transition in the corona from a lateral homogeneous (for low values of χ_{AC}) to a phase segregated corona (above a threshold value of χ_{AC}). The transition was shown to be rather abrupt but not jumplike. For a given micellar concentration (fixed translationally restricted grand potential), we found that below the transition the aggregation number decreases with increasing repulsion between *A* and *C*, whereas above the transition there is an increase in aggregation number. The kink in the curve of $g(\chi_{AC})$ shows that the second derivative of the free energy to the chemical potential is discontinuous, pointing to the second-order phase transition. The interface between *A* and *C* rich phases has several peculiarities. The interface widens with increasing distance from the core. Near the core, a true interface exists with a finite (local) interfacial tension and a small accumulation of solvent between the two phases. In the periphery of the corona, the *A* and *C* chains are only separated because they are forced to be separated near the core. Another peculiarity is that the orientation of the molecules in the *A* and *C* rich phases are parallel to the interface. In the regime of strong segregation, we find that neither the core nor the overall micelle remains perfectly spherical. This is noteworthy because the lengths of the corona blocks were chosen as sufficiently large to prevent nonspherical topology for micelles with a homogeneous corona to form. One of the interesting findings was that the transition from a mixed to segregated corona can be induced by increasing the aggregation number. As the micelle size is a weakly increasing function of the overall micelle concentration, we anticipate that the occurrence of Janus micelles may depend (in some cases) on the polymer concentration in the system. Near the transition point, the first appearance of Janus micelles is accompanied by a weak segregation between the two polymer segments, and diffuse interfaces with an ultralow interfacial tension. In this regime, we expect that thermal fluctuations can disrupt the two-phase structure and induce a multiple domain structure of the corona. For strong segregation, however, the two-face Janus structure should be the ground state.

Appendix I

In this Appendix, we show that the free energy, eq 11, of the system consisting of a triblock terpolymer $A_NB_MC_N$ and a solvent *S* is equivalent to the free energy of a triblock copolymer $A^*_{\tilde{N}}B_MA^*_{\tilde{N}}$ in a solvent. The nonzero interactions between blocks *A* and *C* ($\chi_{AC} > 0$) can be accounted for by using renormalized interaction parameters of the monomer A^* with the block *B* and the solvent. The derivation relies on the *a priori* assumption that the volume fractions of the monomers $\varphi_A(\mathbf{r})$ and $\varphi_B(\mathbf{r})$ are equal to each other at all $\mathbf{r}$ (this is not true for micelles with a segregated corona). As a consequence, structural and thermodynamic properties of the mixed terpolymeric micelles are the same as those of micelles formed by $A^*_{\tilde{N}}B_MA^*_{\tilde{N}}$ copolymers with modified interaction parameters.

The density of the free energy of interactions, eq 12, may be written as a sum of contributions from each pair of monomers

$$f^{\text{int}}(\mathbf{r}) = f_{AS}(\mathbf{r}) + f_{BS}(\mathbf{r}) + f_{CS}(\mathbf{r}) + f_{AB}(\mathbf{r}) + f_{BC}(\mathbf{r}) + f_{AC}(\mathbf{r}) \tag{23}$$

For brevity, below we will drop the spatial coordinates. Each item in the sum has the form

$$f_{xy} = \frac{1}{2}\chi_{xy}\left(\varphi_x\left\langle\varphi_y - \varphi_y^{\text{b}}\right\rangle + \varphi_y\left\langle\varphi_x - \varphi_x^{\text{b}}\right\rangle\right) \tag{24}$$

and due to the symmetry of the triblock and the equal fractions of *A* and *C*, $\varphi_A = \varphi_C$, eq 23 reduces to

$$f^{\text{int}} = 2f_{AS} + f_{BS} + 2f_{AB} + f_{AC} \tag{25}$$

Using the incompressibility condition $\varphi_A + \varphi_B + \varphi_C + \varphi_S = 1$, we eliminate the dependence of f_{AC} on φ_C

$$f_{AC} = -\frac{1}{4}\chi_{AC}\left(\varphi_A\left\langle\varphi_S - \varphi_S^{\text{b}}\right\rangle + \varphi_S\left\langle\varphi_A - \varphi_A^{\text{b}}\right\rangle\right) - \frac{1}{4}\chi_{AC}\left(\varphi_A\left\langle\varphi_B - \varphi_B^{\text{b}}\right\rangle + \varphi_B\left\langle\varphi_A - \varphi_A^{\text{b}}\right\rangle\right) + \frac{1}{4}\chi_{AC}\left\langle\varphi_A - \varphi_A^{\text{b}}\right\rangle \tag{26}$$

The last term is linear in φ_A and therefore does not influence the optimization procedure. The first term of eq 26 can now be included in f_{AS} of eq 25, and the second term of eq 26 can be included in f_{AB} of eq 25, leading to

$$f^{\text{int}} = f_{A^*B} + f_{BS} + f_{A^*B} \tag{27}$$

where f_{A^*S} and f_{A^*B} are defined by eq 24 with $\varphi_{A^*} = \varphi_A + \varphi_C = 2\varphi_A$ and $\chi_{A^*S} = \chi_A - (1/4)\chi_{AC}$ and $\chi_{A^*S} = \chi_{AB} - (1/4)\chi_{AC}$.

The conformational part of the free energy eq 11 is not affected by this substitution.

Acknowledgment. The authors acknowledge financial support from the Dutch National Science Foundation (NWO) and Russian Foundation for Basic Research (RFBR) through the joint project 047.017.026 "Polymers in nanomedicine: design, synthesis and study of interpolymer and polymer-virus complexes in search of novel pharmaceutical strategies". Financial support from the EU POLYAMPHI/Marie Curie program (RT6-2002, Proposal 505027) and European Science Foundation EUROCORES program collaborative BIOSONS is also acknowledged.

References and Notes

(1) Evans D. F., Wennerström, H. *The colloidal domain where physics, chemistry, biology, and technology meet*; VCH Publishers, Inc.: New York, **1994**.
(2) Nagarajan, F.; Ruckenstein, E. *Langmuir* **1991**, *7*, 2934–2969.
(3) Laughlin, R. G. *The aqueous phase behavior of surfactants*; Academic Press: New York, 1994.
(4) Riess, G. *Prog. Polym. Sci.* **1999**, *28*, 1107–1170.
(5) Bates, F. S., Fredrickson, G. H. *Phys. Today*, *52*, 32−38.
(6) Fustin, C. A.; Abetz, V.; Gohy, J. F. *Eur. Phys. J. E* **2005**, *16*, 291–302.
(7) Halperin, A. *J. Phys. (Paris)* **1988**, *49*, 131–137.
(8) Halperin, A. *Macromolecules* **1990**, *23*, 2724–2731.
(9) Erhardt, R.; Zhang, M. F.; Boker, A.; Zettl, H.; Abetz, C.; Frederik, P.; Krausch, G.; Abetz, V.; Muller, A. H. E. *J. Am. Chem. Soc.* **2003**, *125*, 3260–3267.
(10) Saito, R.; Fujita, A.; Ichimura, A.; Ishizu, K. *J. Polym. Sci., Part A: Polym. Chem.* **2000**, *38*, 2091–2097.

(11) Voets, I. K.; de Keizer, A.; de Waard, P.; Frederick, P. M.; Bomans, P. H. H.; Schmalz, H.; Walther, A.; King, S. M.; Leermakers, F. A. M.; Cohen Stuart, M. A. *Angew. Chem., Int. Ed.* **2006**, *45*, 6673–6676. Voets, I. K.; Fokkink, R.; Hellweg, T.; King, S. M.; de Waard, P.; Frederik, P. M.; Bomans, P. H. H.; de Keizer, A.; Cohen Stuart, M. A. This paper contains experimental data on deformations of the core and corona in a complex cocervate core Janus micelle.
(12) Gohy, J. F.; Khousakoun, E.; Willet, N.; Varshney, S. K.; Jerome, R. *Macromol. Rapid Commun.* **2004**, *25*, 1536–1539.
(13) Zhulina, E. B.; Adam, M.; LaRue, I.; Sheiko, S. S.; Rubinstein, M. *Macromolecules* **2005**, *38*, 5330–5351.
(14) Flory, P. J. *Principles of Polymer Chemistry*; Cornell Univesity Press: Ithaca, NY, 1953.
(15) Wijmans, C. W.; Zhulina, E. B. *Macromolecules* **1993**, *26*, 7214–7224.
(16) Li, H.; Witten, T. A. *Macromolecules* **1994**, *27*, 449–457.
(17) de Gennes, P.-G. *Scaling Concepts in Polymer Physics*; Cornell University Press: Ithaca, New York, 1979.
(18) Hong, K. M.; Noolandi, J. *Macromolecules* **1981**, *14*, 736–742.
(19) Hall, D. G.; Pethica, B. A. *Non-ionic surfactants*; Marcel Dekker: New York, 1976; Chapter16.
(20) Israelachvili, J. N.; Mitchell, D. J.; Ninham, B. W. *J. Chem. Soc., Faraday Trans. 2* **1976**, *72*, 1525–1568.
(21) Porte, G. *J. Phys. Chem.* **1983**, *87*, 3541–3550.
(22) Eriksson, J. C.; Ljunggren, S. *Langmuir* **1990**, *6*, 895–904.
(23) Hill, T. L. *Thermodynamics of Small Systems, Parts 1 and 2*; Dover Publications Inc.: New York, 1994.
(24) Fleer, G. J.; Cohen Stuart, M. A.; Scheutjens, J. M. H. M.; Cosgrove, T.; Vincent, B. *Polymers at Interfaces*; Chapman and Hall: London, 1993.
(25) Jódar-Reyes, A. B.; Ortega-Vinuesa, J. L.; Martín-Rodríguez, A.; Leermakers, F. A. M. *Langmuir* **2003**, *19*, 878–887.
(26) Böhmer, M. R.; Koopal, L. K.; Janssen, R.; Lee, E. M.; Thomas, R. K.; Rennie, A. R. *Langmuir* **1992**, *8*, 2228–2239.
(27) Jódar-Reyes, A. B.; Ortega-Vinuesa, J. L.; Martín-Rodríguez, A.; Leermakers, F. A. M. *Langmuir* **2002**, *18*, 8706–8713.
(28) Edwards, S. F. *Proc. Phys. Soc.* **1965**, *95*, 613–624.
(29) Evers, O. A.; Scheutjens, J. M. H. M.; Fleer, G. J. *Macromolecules* **1990**, *23*, 5221–5233.
(30) Daoud, M.; Cotton, C. P. *J. Phys. (Paris)* **1982**, *43*, 531–538.
(31) Leermakers, F. A. M.; Sprakel, J.; Besseling, N. A. M.; Barneveld, P. A. *Phys. Chem. Chem. Phys.* **2007**, *9*, 167–179.
(32) Broseta, D.; Fredrickson, G. H.; Helfand, E.; Leibler, L. *Macromolecules* **1990**, *23*, 132–139.
(33) Futterer, T.; Vliegenthart, G. A.; Lang, P. R. *Macromolecules* **2004**, *37*, 8407–8413.

MA800130Q